Forest thinning impacts on the water balance of Sierra Nevada mixed-conifer headwater basins

P. C. Saksa[1], M. H. Conklin[1], J. J. Battles[2], C. L. Tague[3], and R. C. Bales[1]

[1]Sierra Nevada Research Institute, University of California, Merced, California, USA.
[2]Department of Environmental Science, Policy and Management, University of California, Berkeley, California, USA.
[3]Bren School of Environmental Science and Management, University of California, Santa Barbara, California, USA.

Key Points:
- **Low-intensity forest thinning can increase runoff in the central Sierra Nevada in both wet and dry years**
- **In the southern Sierra, low-intensity forest thinning does not affect runoff, owing to evapotranspiration being more water limited**
- **Distributed measurements of snow and soil moisture can better support spatially explicit modeling than only constraining with streamflow**

Abstract
Headwater catchments in the mixed-conifer zone of the American and Merced River basins were selectively thinned in 2012 to reduce the risk of high-intensity wildfire. Distributed observations of forest vegetation thinning, precipitation, snowpack storage, soil-water storage, energy balance and stream discharge from 2010 to 2013 were used to calculate the water balance and constrain a hydro-ecologic model. Using the spatially calibrated RHESSys model, we assessed thinning effects on the water balance. In the central-Sierra American River headwaters, there was a mean annual runoff increase of 14% in response to the observed thinning patterns, which included heterogeneous reductions in Leaf Area Index (-8%), canopy cover (-3%), and shrub cover (-4%). In the southern-Sierra Merced River headwaters, thinning had little impact on forest structure or runoff, as vegetation growth in areas not thinned offset reductions from thinning. Observed thinning effects on runoff could not be confirmed in either basin by measurements alone, in part because of the high variability in precipitation during the measurement period. Modeling results show that when thinning is intensive enough to change forest structure, low-magnitude vegetation reductions have greater potential to modify the catchment-scale water balance in the higher-precipitation central Sierra Nevada versus in the more water-limited southern Sierra Nevada. Hydrologic modeling, constrained by detailed, multi-year field measurements, provides a useful tool for analyzing catchment response to forest thinning.

1. Introduction
The movement of water through mountain catchments in the western United States depends on the interaction of climate, vegetation, and subsurface processes. Characterizing these components, and their influence on snowpack and water supply, is a priority for effective management of land and water resources. The major land manager in the Sierra Nevada, the U.S. Forest Service, routinely undertakes vegetation treatments to reduce the risk of large high-intensity wildfires and restore forests to more sustainable states. Vegetation density in these forests is high compared to a century ago [*Collins et al.*, 2011], and thinning prescriptions range from low-intensity Strategically Placed Landscape Treatments [*Finney*, 2001] to more-intensive restoration treatments [*North et al.*, 2007; *Wayman and North*, 2007].

Forest management to encourage fire-resilient landscapes also impacts the hydrology. Typical treatments include prescribed burning and selective thinning to reduce surface and ladder fuels and lower crown density, while maintaining larger fire-resistant trees [*Agee and Skinner*, 2005]. The magnitude and pattern of vegetation removal affect snow interception [*Storck et al.*, 2002] and melt [*Essery et al.*, 2008], water use by vegetation [*Whitehead et al.*, 1984; *Whitehead and Kelliher*, 1991; *Moore et al.*, 2004], and thus runoff [*Ffolliott et al.*, 1989; *Zou et al.*, 2010]. In addition, reviews of more than 90 catchment studies of treatment effects on streamflow [*Stednick*, 1996; *Bosch and*

Hewlett, 1982] note the importance of post-treatment precipitation and the rate of vegetation regrowth on the run-off response to the treatments.

Changes in forest vegetation density from growth or disturbance can also influence catchment-scale canopy interception rates and the magnitude of energy inputs to the seasonal Sierra Nevada snowpack. *Kittredge* [1953] developed linear relationships between precipitation and interception rates in forests with different canopy cover and found an increase in the interception slope coefficient with increases in canopy cover, which indicated greater interception capacity in high-precipitation events. Forest cover affects surface energy input to the snowpack on the ground by reducing surface shortwave radiation and increasing longwave radiation [*Essery et al.*, 2008]. The resulting snowmelt rate and timing can have a significant influence on the routing and volume of precipitation moving through a catchment. In regions with warm winters, such as the mid-elevation Sierra Nevada, *Lundquist et al.* [2013] suggest that reduced canopy cover decreases mid-winter and early-spring snowmelt. This effect is in fact a result of the smaller influence of shortwave energy from the low-angle winter sun in open areas and the greater influence of longwave energy in areas of forest cover from the warmer temperatures. Analyzing the specific relationship between forest gap size and net radiation, *Lawler and Link* [2011] compared the magnitude of incoming all-wave radiation at an Idaho forest with gap sizes of 1 to 6 tree heights (25-150 m), and determined that net radiation is lowest in gaps of 1 to 2 tree heights (25-50 m). They also showed that net radiation starts to exceed open-area radiation in the northern portions of gaps 3 tree heights (75 m) and larger, where combined rates of shortwave and longwave energy from vegetation are highest.

Catchment-scale transpiration response to forest thinning depends on regional precipitation amounts and the rate of understory or overstory vegetation regrowth following treatments. *Zhang et al.* [2001] used empirical relationships developed from catchment water-balance studies worldwide to estimate the increasing response of evapotranspiration to changes in forest cover with increasing annual precipitation. Considering forested watersheds across the conterminous United States, *Sun et al.* [2015] used the Water Supply Stress Index model to calculate a potential range of water yield increases of 0-63% with a 50% reduction in leaf area index (LAI). *Biederman et al.* [2014] showed that reduced transpiration in disturbed forests may not always lead to expected streamflow increases, and can be offset by increased evaporation and sublimation.

The key management question remains the extent to which reductions in biomass increase runoff in specific forests. *Marvin* [1996] applied multiple regressions of runoff response to percent forest cover reduction, mean annual precipitation, mean annual runoff, and runoff fraction from 31 experimental catchments in the western United States to project treatment effects in the Sierra Nevada. Her results predicted that a 10% reduction of canopy cover in mixed conifer forests would have no statistically significant effect on annual runoff (-0.2-1.2 cm). She further argued that it is more difficult to determine effects of treatments on runoff in the semi-arid West than in the set of catchments analyzed by *Bosch and Hewlett* [1982]. Using existing literature, *Kattelmann et al.* [1983] concluded that removing all vegetation in the Sierra Nevada could increase runoff 30-40%, while managing National Forest land specifically for water production could increase runoff by 2-6%. However, they noted that limitations on management (*e.g.*, inability to access steep slope, wildlife protection zones, and prohibitive costs) lower this estimate to about 0.5-2% (0.3-1.2 cm). Instead of an increase in runoff, they suggested that the hydrological benefit of treatments is a delay in snowpack ablation.

Models for projecting runoff response to vegetation changes are often constrained by discharge alone [*Corbari et al.*, 2015]. However, there has also been a concerted effort for continued field studies and increased observational data to adequately support modeling efforts [*Dunne*, 1983; *Grayson et al.*, 1992; *Silberstein*, 2006; *Burt and McDonnell*, 2015]. *Grayson et al.* [2002] promote the comparison of observed and modeled spatial patterns, suggesting examples of explicit catchment snow, soil moisture, and runoff characterizations, in order to avoid getting the right results for the wrong reasons [*Klemes*, 1986 in *Grayson et al.*, 2002]. While a number of long-term research catchments have provided a wealth of information on forested, mountain hydrology [e.g. *Hicks et al.*, 1991; *Swank et al.*, 2001; *Troendle et al.*, 2001; *Chauvin et al.*, 2011], there have been few experimental catchment

studies in the Sierra Nevada [*Hunsaker et al.*, 2012]. The objectives of this study were to: *i*) measure the water balance in central and southern Sierra Nevada mixed-conifer headwater catchments across a range of annual precipitation amounts, *ii*) calibrate and evaluate a well-constrained hydrologic modeling tool using observations of multiple water-balance components, and *iii*) apply the constrained model to evaluate catchment hydrologic response to forest thinning currently used by land managers.

2. Methods

The water balances across two headwater catchments in the central-Sierra American River basin (American R.) and two in the southern-Sierra Merced River basin (Merced R.) were monitored to inform assessments of fuels treatments and wildfire on evapotranspiration and runoff in these areas (Figure 1) [*Conklin et al.*, 2015]. The four catchments (1.4-2.2 km^2 each) are in the high-density, mixed-conifer zone, and were monitored over four water years (October 1, 2009 to September 30, 2013). One catchment in each area was thinned for fuels reductions beginning in fall 2011, with most of the vegetation removal occurring in fall 2012. However, the thinning prescriptions for fuels reduction were relatively low intensity, resulting in small biomass removals. Vegetation was surveyed before and after thinning. Water-balance measurements were used to evaluate the catchment hydrologic responses to the highly variable seasonal and interannual climate. Data for the two treated catchments were integrated using the spatially explicit Regional Hydro-Ecologic Simulation System (RHESSys) to assess the effects of the fuels treatments on the seasonal and interannual water balances. We focused model calibration and evaluation on the two treated catchments. Our calibration approach used multiple components of the catchment water balance (snow accumulation, snowmelt, and streamflow) for three years. For model evaluation, these same components were used in the fourth year, plus additional water balance elements (soil water storage and evapotranspiration) over all four years. The two untreated catchments were used to assess the consistency of the water balance across forested headwater catchments in each study area.

2.1 Site characteristics

The Mediterranean climate of the Sierra Nevada is characterized by cool wet winters and warm dry summers. Study catchments are in the transition zone from rain- to snow-dominated precipitation, with winter snowpack intermittent at lower elevations and persistent higher up. Mean winter and summer temperatures are about 4 and 18^oC, respectively. The Bear Trap Creek (1.4 km^2) and Frazier Creek (1.8 km^2) catchments are in the American R. basin, with Big Sandy Creek (2.2 km^2) and Speckerman Creek (1.9 km^2) are in the Merced R. basin. Elevations range from 1560 to 2475 m.

Subsurface bedrock in the American R. catchment of Bear Trap is dominated by the Shoo Fly Complex, composed of metasedimentary sandstone and shale, and in Frazier Creek the underlying bedrock is dominated by volcanic pyroclasts [*Saucedo and Wagner*, 1992]. In the Merced R., both catchments have similar bedrock compositions of granodiorite batholith [*Bateman*, 1989]. In the American R. headwater catchments, it is assumed that streams are fed by surface and shallow subsurface sources; however the groundwater component of volcanic deposits can be deeper [*Tague and Grant*, 2004]. Water in Merced R. tributary streams comes from recent surface and shallow groundwater [*Shaw et al.*, 2014].

Soils in the American are well drained, with Bear Trap having the Crozier-Cohasset, Crozier-McCarthy-Cohasset, and Hurlbut-Deadwood complexes and Frazier having the Crozier-Cohasset, Crozier-McCarthy-Cohasset, and Crozier-Mariposa-Cryumbrepts complexes [*Soil Survey Staff*, 2011]. Merced soils are also well drained, with Speckerman having Ledford family-Entic-Xerumbrepts and Chaix-Chawanakee families, and Big Sandy having Ledford-family Entic Xerumbrepts and Umpa-family soil series [*Soil Survey Staff*, 2011]. Soil samples were collected at all 128 moisture-sensor locations and analyzed for texture. Nearly all of the soils contained greater than 50% sand, and they all contained less than 50% silt and 30% clay. Soils in the American were classified as loam or sandy loam, and soils in the Merced were sand or sandy loam. Textures were more variable between individual sensor locations than between sensor depths (30-60 cm) below the surface.

Forest-plot vegetation surveys showed 48% canopy cover, 31 $m^2\,ha^{-1}$ basal area, and 43% shrub

cover in the American catchments, with respective values for the Merced being 70% canopy cover, 56 $m^2 ha^{-1}$ basal area, and 26% shrub cover [*Fry et al.*, 2015]. Mixed-conifer forest in the American sites is dominated by white fir (*Abies concolor*) and Douglas-fir (*Pseudotsuga menziesii*), with an understory of manzanita (*Arctostaphylos spp.*). Mixed-conifer in the Merced sites is dominated by white fir and incense cedar (*Calocedrus decurrens*), with understory shrub species including mountain whitethorn (*Ceanothus cordulatus*), deerbrush (*Ceanothus integerrimus*), and greenleaf manzanita (*Arcostaphylos patula*).

2.2 Water-balance measurements

Meteorological stations in the upper and lower elevations of each set of catchments recorded hourly precipitation, snow depth, temperature, wind speed and direction, and radiation for the entire period of this study (Figure 1). The unshielded tipping-buckets deployed in the catchments only accurately measured precipitation from rain. So quantitative daily precipitation amounts for model input were acquired from nearby operational stations having the capability of consistently measuring both rain and snow events. At the American River sites, precipitation data were taken from the Blue Canyon meteorological station (1610 m), operated by the U.S. Bureau of Reclamation, 22 km to the northeast and similar in elevation to the lower meteorological station. In the Merced River site, precipitation data from the U.S. Bureau of Reclamation Poison Ridge meteorological station (2100 m) were used, which is 8 km to the southeast and similar in elevation to the upper meteorological station. Interannual differences in precipitation from these gauges were consistent with long-term indexes reported by the California Department of Water Resources, where the mean of multiple stations is used as a relative index of regional precipitation. The 8-station Northern California Precipitation Index was at 63% (2012) to 145% (2011) of the long-term mean (1922-1988) and the 5-station Southern California Precipitation Index was 61% (2012) to 160% (2011) of the mean (1956-2005).

Distributed ultrasonic snow-depth sensors (Judd Communications; 15 each for the American and Merced study areas) and co-located soil-moisture sensors (Decagon ECHO-TM; 64 for each site) provided continuous hourly measurements over a range of elevation, slope, aspect and forest cover, similar to *Bales et al.* [2011]. For each study area, snow-depth sensors were installed on the north-facing slope (2-3 sensors) and the south-facing slope (2-3 sensors) adjacent to the upper and the lower meteorological stations. Additional sensors were installed on the north-facing slope (1-2 sensors) and south-facing slope (1-2 sensors) adjacent to the thinned catchment outlet and not thinned catchment outlet. Observed snow depth was converted to snow water equivalent (SWE) using a linear relationship between the day of year and snowpack density from the nearest snow pillow at similar elevation [*Liu et al.*, 2013]. Soil-moisture sensors were also installed on the north-facing slope (8 sensors) and south-facing slope (8 sensors) at the upper and lower meteorological stations and each catchment outlet. The sensors were split into pairs at the four cardinal directions around a conifer tree, installed at 1-m distance out from the trunk, at depths of 30 and 60 cm below the surface.

Stream stage was recorded at each catchment outlet by pressure-sensitive depth recorders. Stream discharge was measured using the salt-dilution method [*Moore*, 2013] to develop a stage-discharge rating curve. Discharges were measured over a range of flows during the four years, with a minimum of 16 data points available. A majority of measurements were at low to medium stream discharge (Figure S1). Higher flows thus have greater uncertainty, consistent with previous reports in small catchments where there is a short measurement time to capture the flashy discharge [Westerberg *et al.*, 2016]. Over the four years, 93% to 99% of the stream discharge volume occurred within the range of measured discharge used for calculating the rating curves (Figure S1), with much of the higher flow being in 2011.

2.3 Vegetation characteristics

LiDAR and color-infrared aerial imagery data collected before the fuels-reduction were used to define polygons of similar aspect, slope position, and vegetation composition, vertical structure, basal area, and canopy cover [*Su et al.*, 2016]. Bear Trap had 28 polygons, 19 covering >1% of the catchment, and the largest covering 9.6% of the area. Big Sandy had 32 polygons, 19 covering >1% of the catchment, and the largest polygon covering 13.9%. Polygons covering <1% of the catchment areas were located along ridges, and extended into

adjacent catchments. Detailed vegetation attributes (canopy cover, leaf area index, and shrub cover) for each polygon were developed from vegetation plots sampled before and after thinning, involving over 1000 individual trees (American, n=1363; Merced, n=1100) [*Fry et al.*, 2015]. An imputation procedure was developed to assign these field plots to each map polygon based on their similarity in "gradient space", defined using multivariate analysis [*Ohmann and Gregory*, 2002]. To recreate the fine-scale heterogeneity observed in the field, all plots ranked in the 95th percentile in terms of similarity to a polygon were identified, and three were randomly assigned to the polygon. Variables included treatment type, vegetation type, canopy cover, relative density of big trees, and a suite of topographic metrics.

Bear Trap was completely covered by the mature mixed-conifer classification and Frazier was 95% mature mixed conifer, 3% young mixed conifer, and 2% cedar forest. Speckerman contained 82% mature mixed conifer with 18% live oak-pine forest and Big Sandy was covered by all vegetation types at 56% mature mixed conifer, 33% live oak-pine, 6% open pine-oak woodland, and 5% closed-canopy conifer forest.

Canopy cover was defined as the percentage of the ground area that is directly covered with tree crowns, calculated according to *Crookston and Stage* [1999] using regional allometric equations that estimate projected crown area as a function of species and diameter at breast height (dbh, breast height = 1.37 m). Cover estimates were corrected for canopy overlap. Leaf area was also calculated from species-specific allometric models based on a robust sampling of the dominant species in the catchments [*Jones et al.*, 2015]. The projected leaf area of the all the trees was summed and then divided by the plot area to calculate LAI. Shrub cover was calculated in each vegetation community type from the forest-plot measurements:

$$SC_{\text{American}} = 63.079 - 0.244BA - 0.257CC \quad [1]$$

$$SC_{\text{Merced}} = 55.273 - 0.294BA - 0.256CC \quad [2]$$

where *SC* is shrub cover, *BA* is basal area (m^2 ha^{-1}) and *CC* (%) is canopy cover. The low coefficients of determination (R^2 = 0.16 for American and 0.25 for Merced) were a result of the highly scattered relationships, but the equations are functionally relevant where higher-density vegetation and overstory cover produces lower predicted shrub cover. In polygons where the overstory was thinned, shrub cover was held constant, as the understory growth response would not be instantaneous. In hydrologic modeling, we assumed that the relationships defining overstory and understory structure were constant in all scenarios.

2.4 Hydrologic modeling

RHESSys combines a meteorological-forcing model (MTNCLM, [*Hungerford et al.*, 1989]), an ecosystem carbon and nutrient cycling model, and a spatially distributed hydrologic-routing model that accounts for both vertical and lateral water fluxes. RHESSys algorithms are continuously updated to reflect improved process representation; in this project we used version 5.14.7. The model has been previously applied in a variety of snow-dominated mountain catchments to examine climate and land-cover change impacts. Comparisons with observations at these sites show good correspondence between model estimates and observations of streamflow (*e.g. Tague and Peng*, 2013; *Tague et al.*, 2013), ecosystem fluxes through tree rings [*Tague et al.*, 2013; *Vicente-Serrano et al.*, 2015], and flux-tower data [*Zierl et al.*, 2007]. The catchments that were not thinned provided a second observation point of annual water balance components in catchments of similar size and vegetation type.

Input to RHESSys requires extensive spatial data, and we used a 20-m DEM, soil layer from the SSURGO database [*Soil Survey Staff*, 2011], and the vegetation layer described above. Patches are the smallest unit of vegetation and soil representation in the model used for calculating hydrologic processes. Model patches were created using the r.clump module in GRASS GIS (GRASS 6.4.4), which produces spatially contiguous areas of similar elevation and slope based on the DEM. Bear Trap had 3213 model patches and Big Sandy had 4448 patches, at least 75% of patches in both catchments were at the native DEM resolution of 400 m^2, with a maximum patch size of 18,400 m^2 (46 pixels). Individual patch vegetation and soil characterization is determined from the overlapping vegetation polygon and soil type.

RHESSys also requires precipitation, minimum temperature, and maximum temperature at a daily time-step. Precipitation input is typically a single

amount, with the model estimating the amount of rain or snow based on a linear transition from rain to snow over a user-defined temperature range (*i.e.* -2 to 2°C). Because individual storms had variable temperatures that impacted precipitation phase in these rain-snow transition elevations, we instead specified separate rain and snow events at each meteorological station. We used a binary process where an increase in daily snow depth recorded by the installed sensors defined a snow event, otherwise it was defined as a rain event. The specified snow and rain events replicated the observed snow accumulation and melt pattern more accurately than the model estimate of precipitation phase based on air temperature.

We used two climate zones in the model for the upper and lower climate stations, and both of the modeled catchments had a mean wintertime temperature (Nov-Apr) of 4.3°C, but 40% of precipitation was snow in Bear Trap versus 60% in Big Sandy, reflecting its higher elevation range. The distribution of precipitation phase across each zone is adjusted from the elevation of the meteorological station using standardized lapse rates in the model, as snowpack patterns were not sensitive to lapse rates calculated separately using the meteorological stations. Summer (May-Oct) mean daily temperature was 18.3°C in Bear Trap and 17.8°C in Big Sandy. The respective mean elevations for Bear Trap and Big Sandy are 1723 m and 2140 m, with respective ranges of 1619-1826 m and 1808-2473 m. The standardized lapse rate of 6.5°C km^{-1} [*Barry and Chorley*, 1987] suggests that if these basins were co-located, Big Sandy would be 2.7°C cooler than Bear Trap, but the lower latitude of Big Sandy results in more comparable temperatures between the catchments.

Modeled snowmelt in RHESSys [*Coughlan and Running*, 1997] is estimated using a quasi-energy budget calculation

$$q_{melt} = M_T + M_{rad} + M_V \quad [3]$$

where M_T is melt due to sensible and latent heat

$$M_T = \beta_{MT} T_{air}(1 - 0.8F) \quad [4]$$

M_{rad} is melt from radiation

$$M_{rad} = \frac{\beta_{Mrad}(K_{direct} + K_{diffuse} + L)}{\lambda_f \rho_{water}} \quad [5]$$

and M_V is melt from advection [*Tague and Band*, 2004].

$$M_V = \frac{\rho_{water} T_{air} TF cp_{water}}{\lambda_f} \quad [6]$$

In these equations β_{MT} is an empirical temperature melt coefficient (m °C^{-1}), T_{air} is the mean daily air temperature (°C), F is the fractional canopy cover over the snowpack, β_{Mrad} is an empirical radiation melt coefficient (m kJ^{-1} m^2 day^{-1}), K_{direct} is the direct shortwave radiation, $K_{diffuse}$ is the diffuse shortwave radiation, L is the longwave radiation, λ_f is the latent heat of fusion, ρ_{water} is the density of water, cp_{water} is the heat capacity of water, and TF is throughfall into the snowpack. Melt only occurs when the snowpack is isothermal (snow temperature is uniformly 0°C); otherwise sublimation occurs, and the latent heat of vaporization (λ_v) is added to the latent heat of fusion.

The empirical radiation melt coefficient in equation 5 was added after the original radiation calculation was published by *Tague and Band* [2004], to provide an index-based temperature and radiation calculation of snowmelt, similar to the approach of *Brubaker et al.* [1996] used by *Cornwall et al.* [2016]. Energy input to the snowpack is affected by both LAI and canopy cover, which are described in equations 19-26 from *Tague and Band* [2004]. The radiation coefficient only impacts snowmelt, and does not affect incoming radiation or the amount of radiation intercepted by vegetation. The need for this coefficient was apparent in the current modeling versus prior implementations of RHESSys, as distributed snow observations were part of the calibration.

Snowmelt in RHESSys was calibrated by comparing the model estimate of basin-scale snowpack to an elevation-adjusted observed snowpack based on the spatially distributed, strategically placed sensors. We assumed a constant rate of increase in snowpack depth with elevation between the lower and upper meteorological stations to estimate the snowpack at the mean catchment elevation. This optimization approach was used to constrain snowpack independently of streamflow, and helps account for the heterogeneity of LAI and canopy cover within the vegetation polygons, which can result in a non-linear snowmelt response compared to the polygon mean values. Snowmelt parameters were optimized by minimizing the mean average error of the simulated and observed snowpack: all catchments used a radiation melt coefficient (β_{Mrad}) of 0.4, and

individual temperature-snowmelt coefficients (β_{MT}) of 0.0005 for Bear Trap, 0.0003 for Frazier, and 0.001 for Big Sandy and Speckerman. Compared to the original snowmelt model [*Coughlan and Running*, 1997], temperature melt coefficients for Bear Trap and Frazier are lower, but Big Sandy and Speckerman have the same coefficient value. Another Sierra Nevada RHESSys study at a similar elevation range using LiDAR-derived vegetation input reported a higher melt coefficient of 0.005 [*Son et al.*, 2016].

After manual calibration of snowpack, streamflow was calibrated using a Monte Carlo-based method with 5000 normally distributed random parameter sets (Table 1). Parameters controlling soil physical properties of pore-size index (*po*) and air-entry pressure (*pa*), along with parameters controlling flow properties of vertical and lateral hydraulic conductivity at the surface (*k, svk,* respectively), decay of hydraulic conductivity with depth (*m*), and percent of infiltrated water lost through fracture flow to deep groundwater (*gw1*) and deep-groundwater drainage rate (*gw2*) were optimized in the calibration process. Acceptable parameter sets were determined by comparing observed and modeled daily stream discharge, and we used multiple assessments to quantify model accuracy, similar to the calibration approach of previous studies [*Garcia et al.*, 2013; *Garcia and Tague, 2015*; *Son et al*. 2016]. Minimum calibration criteria included a Nash-Sutcliffe Efficiency (NS_e; Nash and Sutcliffe, 1970) of daily streamflow and Nash-Sutcliffe Efficiency of log-transformed daily streamflow ($logNS_e$) that were required to be greater than 0.60, in order to capture both the daily discharge and seasonal trends of high winter flows and low summer flows that are typical of a Mediterranean climate. Simulated discharge was also required to be within 20% of measured annual flows and within 25% of measured August flows to constrain the annual water balance and summer baseflow. Modeled water balance was assessed using surface runoff, evapotranspiration, and subsurface bypass flow. Bypass flow is used in RHESSys as a comprehensive term for all subsurface storage and routing, and is the amount of precipitation not attributed to runoff or evapotranspiration.

3. Results

3.1 Water-balance measurements

Annual precipitation during the study period varied considerably in California and the Sierra Nevada: 2010 was an average precipitation year, 2011 was a very wet year [*Guan et al.*, 2013], and 2012-2013 were the first two years of an extended drought [*Griffin and Anchukaitis*, 2014; *Asner et al.*, 2015]. Measured annual runoff in the American catchments (41-167 cm) was higher than in the Merced (23-112 cm), reflecting the higher precipitation of the more-northern sites. Within the American R., the Frazier Creek catchment consistently had higher runoff than did Bear Trap in the pre-thinning years of 2010-2012 (Figure 2, Table 2). Runoff in 2013 was similar in Frazier and Bear Trap. Within the Merced R., runoff in the Speckerman catchment was 70-75% of that in in Big Sandy for the wetter years of 2010-2011, but runoff in the drier years of 2012-2013 was the same in both catchments.

Runoff ratio, the fraction of annual precipitation leaving the catchment as runoff, was highest in the wet 2011, and lowest in the 2nd dry year (2013) in the American catchments (Table 2). In the Merced catchments, runoff ratio was also highest in the wettest year of 2011, but was lowest in the 1st dry year (2012).

Observed streamflow patterns among the four years reflect the variability of precipitation timing and amount, which also influenced the cumulative amount of runoff (Figure 3). In the American catchments, Frazier Creek runoff parallels that for Bear Trap for the first four to five months of the water year, after which runoff in Frazier is higher for the remainder of the snowmelt period. In the Merced, the observed streamflow timing is similar between Big Sandy and Speckerman, but with cumulative runoff higher for Big Sandy for only the first two years (2010-2011).

Soil-moisture values increased with fall rain events, which often occurred in the first month of the water year (Figure 4). Moisture values typically showed sustained saturation through the winter from a combination of intermittent rain events, snowmelt, and low evapotranspiration. Soils in the top 1 m stored 20-30 cm of water during the wet winter season in the Merced catchments, while soils in the American catchments stored 25-35 cm, possibly reflecting the lower sand content. Soil-water storage recession started as early as day 200

in the dry years, but as late as day 270 in the wet year, and directly coincided with observed snowpack melt-out dates. Despite the low precipitation in 2012 and 2013, a combination of drier ridge and hillslope soil moisture combined with summer storms that maintained higher soil moisture in the riparian zone, resulted in a greater soil-storage standard deviation at both sites, and higher summer mean soil storage overall in the American River catchments.

3.2 Modeled forest-treatment effects on water balance

Calibration for the treated catchments of Bear Trap and Big Sandy was completed for water years 2010-2012, as all three years exhibited substantially different precipitation amounts. From the 5000 parameter sets tested, 6 sets for Bear Trap and 17 sets for Big Sandy met the streamflow-performance criteria described above (Table 1, Figure 4). Water year 2013 was post thinning and not used for calibrations, resulting in somewhat lower NS_e (0.34-0.74, 0.27-0.75) and log NS_e (0.68-0.79, 0.29-0.81) for Bear Trap and Big Sandy, respectively, compared to the calibration years (Table 1). All the acceptable parameter sets were used to model the catchments and to calculate a 95% confidence interval. Thinning effects on the catchment water balance were assessed by modeling the vegetation conditions before and after thinning over all four observation years to determine impacts over a range of precipitation and vegetation water availability.

Snowmelt parameters were optimized by minimizing the mean average error of simulated and observed snowpack. The modeled snowpack in Bear Trap represented observations in 2010 and 2013, but underestimated snowpack in 2012 and the accumulation period in 2011 (Figure 4). Optimization of the snowmelt radiation coefficient to 0.4 resulted in the Mean Average Error of 3.1 cm, with higher simulation errors resulting from coefficients of 0.3 (4.7 cm) or 0.5 (3.9 cm). Respective R^2 values were 0.82, 0.69 and 0.83. In Big Sandy, the modeled snowpack matched the 2010 observations, but underestimated the mid-season snowpack in 2011 and 2012 melted somewhat slower in 2013. Optimization of the snowmelt radiation coefficient to 0.4 also resulted in the lowest mean average error (3.1 cm), with higher simulation errors for coefficients of 0.3 (3.5 cm) or 0.5 (4.5 cm). R^2 was 0.89 for all 3 cases.

Modeled root-zone soil storage and streamflow-recession timing depended on snowpack melt-out date and summer storms. Simulation of melt-out dates that were later than observed at both sites in 2010 and at Bear Trap in 2011 propagated to late simulation of soil-water and streamflow recession. Confidence intervals were wider in Big Sandy than in Bear Trap, even with the higher number of simulations. Modeled soil-water storage was most similar to observations in the dry 2012 and 2013 years, with wetting-up and drying-out periods that were often delayed compared to observations. During the wettest year of 2011 in Big Sandy, the model showed elevated moisture content relative to observations in the top meter of soil because soil infiltration exceeded drainage rates in the model, but not in observations. Simulated discharges often replicated the rapid response to specific storm or melt events, but did not recess as quickly as observed from peak flows. The modeled slopes of the soil-water storage and streamflow-recession curves were less steep than observed, possibly reflecting subsurface heterogeneity not captured in the model.

In spite of these limitations in model performance, the model captured major differences between the two sites and between years. Model performance was also similar to that found in other model-based studies of streamflow response to environmental change in the California Sierra Nevada (*e.g. Luo et al.*, 2013).

The mean annual water-balance values (± 95% confidence intervals) for the 4 years showed that in Bear Trap the average 199 cm of precipitation was partitioned into 87 ± 4.5 cm runoff, 74 ± 1 cm transpiration, and 19 ± 2 cm evaporation, with the remaining 19 ± 1 cm routed to subsurface bypass flow. Sublimation was 2.6 cm of the evaporation. In Big Sandy, which averaged 130 cm precipitation, the water-balance values were 60 ± 2 cm runoff, 44 ± 0.4 cm transpiration, 14 ± 0.3 cm evaporation, and 12 ± 0.1 cm subsurface bypass flow. Sublimation was 0.7 cm of the evaporation. Modeled evaporation was similar to the 14 cm interception loss measured by *Rowe and Hendrix* [1951] near Bass Lake, close to Big Sandy.

Model results of the forest thinning that included estimated reductions in both canopy and understory cover resulted in an 8.0% overall LAI reduction in Bear Trap, with thinning in 91% of the catchment, and no overall LAI changes within Big Sandy, with

thinning in 33% of the catchment. The small reductions in vegetation from the fuels reduction in Big Sandy were offset by increases in vegetation in other parts of the catchment over the 5 years (2007-2013) between forest plot measurements.

Thinning in Bear Trap reduced LAI from 9.9 to 9.1. Values in Big Sandy were 6.6 both before and after thinning, but the post-thinning vegetation included relatively more shrubs than trees. was composed of more shrub relative to overstory. Thinning increased runoff in Bear Trap by 14 cm (21%), from 64 ± 5 cm to 78 ± 7 cm during the driest year (2013). During the wettest year (2011), thinning increased runoff by 13 cm (9%), from 147 ± 5 cm to 160 ± 8 cm. Over the 4 years (2009-2013), mean annual runoff increased 12 cm (14%), from 87 ± 5 cm to 99 ± 8 cm (Figure 5). Simulated runoff was 15-20% higher than observed, with measured runoff during the dry, wet, and average years at 54, 126, and 76 cm, respectively. Simulated changes in runoff and evapotranspiration exceeded the 95% confidence interval from the 6 parameter sets and were consistent in dry to wet precipitation conditions, adding 12-14 cm of annual runoff and reducing evapotranspiration by 11-12 cm. Simulated runoff and evapotranspiration did not exceed the 95% confidence interval from the 17 parameter sets in Big Sandy, associated with the light thinning, where overall LAI remained the same, canopy cover increased 1.1%, and shrub cover increased 7.2%.

Using the model results from 2010 (an average precipitation year) at Bear Trap, the changes in storage and fluxes between the pre- and post-thinning vegetation conditions can be compared. Thinning resulted in a deeper modeled snowpack during the accumulation period, reflecting less canopy interception; but the snow melted more quickly during spring ablation owing to the increased energy input to the snowpack (Figure 6). Runoff increased largely during winter and spring, with decreases in evapotranspiration centered around the summer months. Soil-water storage also increased during the summer months in response to the reduction in evapotranspiration.

We also tested the hydrologic model on Frazier and Speckerman (catchments that were not thinned). However, in those two catchments the measured snowpack accumulation and ablation, and the model simulated snowmelt and streamflow, failed to match the timing of measured discharge and peak flows. That is, none of the parameter sets met the minimum calibration criteria for these two catchments. The distributed point snow measurements in these catchments were limited to the extreme upper and lower elevations of the basins, and may not have captured the mean basin response in the highly variable snowpack that occurs across a catchment that transitions from rain- to snow-dominated precipitation.

4 Discussion

4.1 Observed effects of thinning on water balance

The water balance in the catchments that were thinned was compared to the water balance in the catchments that were not thinned to evaluate the impacts of vegetation change. Differences in post-thinning observed runoff between the two American River catchments (Figures 2, 3) could in part reflect forest thinning, but may also reflect differences in subsurface storage due to bedrock differences. Between 2012 (pre-thinning) and 2013 (post-thinning), precipitation increased 5%, and the Bear Trap runoff increased 5%, but the Frazier runoff decreased 29%.

The sum of annual evapotranspiration and change in subsurface storage was calculated as a loss term using precipitation minus runoff (Figure 2, Table 2). In the American R. catchments, this value was 119-141 cm in Bear Trap and 98-125 cm in Frazier, with no consistent pattern between the wet versus dry years. That is, vegetation was apparently not water limited in 2012-2013, even though precipitation declined significantly. The differences in the changes in loss terms from wet to dry years in Bear Trap versus Frazier may reflect differences in regolith properties. Subsurface bedrock in Bear Trap, metasedimentary sandstone and shale, has high flow rates and low potential for storage [*Saucedo and Wagner*, 1992], while the volcanic pyroclasts in Frazier Creek can have a range of behaviors that can include high potential storage and low flow rates depending on the amount of weathering [*Tague and Grant*, 2004].

Daily streamflow that was less than an area-normalized discharge of 0.1 cm was defined as baseflow for the study catchments. Bear Trap discharge was higher than baseflow for 56, 77, 22 and 28% of the year in 2010-2013, respectively, similar to the respective values for Frazier of 50, 63, 23 and 34%. The higher value in 2013 for Frazier could reflect volcanic pyroclasts having

greater regolith water storage; the lower storage potential of the more granitic Bear Trap could then ultimately result in a greater sensitivity to multi-year droughts. The Bear Trap Creek metasedimentary bedrock, with lower storage potential, would more likely show a response to precipitation variability in the same year, without the overlapping multiple-year effects of Frazier Creek. Thus the larger runoff losses observed in Frazier compared to Bear Trap could be the result of a combination of multiple drivers, including a second year of low precipitation, the dry antecedent conditions in 2013, higher transpiration demand from the untreated catchment, or more precipitation being routed into subsurface storage that was already depleted from the first dry year. The differences in the interannual period of higher discharge and baseflow, combined with greater uncertainty in observed discharge during the higher flows, likely contributed to the changes observed between the American catchments.

In the Merced catchments, precipitation minus runoff was similar to the American values in 2010-2011 (90-125 cm), reflecting similar vegetation densities, but dropped significantly in the dry years of 2012-13 (54-60 cm). Although tree mortality was not monitored in Big Sandy and Speckerman beyond the summer of 2013, this decline in precipitation minus runoff coincides with the widespread tree mortality in the southern Sierra Nevada observed in 2014 and subsequent drought years (https://www.fs.usda.gov/detail/r5/forest-grasslandhealth). Geophysical characterization of granitic terrain [*Holbrook et al.,* 2014] and broader spatial scaling of annual evapotranspiration using remotely sensed data [*Fellows and Goulden,* 2016] indicate the potential for subsurface water storage to sustain forest vegetation through multi-year dry periods in some parts of the southern Sierra Nevada, however the observed mortality also suggests that some areas lack sufficient storage. In the Merced R. study area, both Big Sandy and Speckerman catchments responded similarly in the post-thinning dry year, with both having underlying bedrock composed of granodiorite batholith.

High variability in annual precipitation and low post-thinning precipitation resulted in the inability to specifically attribute the changes observed in stream discharge to the fuels reduction. *Bosch and Hewlitt* [1982] note that streamflow response to forest treatments depends on mean-annual precipitation and treatment-year precipitation. Long-term post-disturbance monitoring would be needed to confirm some of the changes in runoff characteristics, as *Troendle and King* [1985] found increases in peak streamflow decades after a forested catchment was harvested that were not detectable shortly after treatments.

4.2 Modeled effects of thinning on water balance

The 14% increase in mean annual runoff and commensurate decrease in evapotranspiration from the fuels treatment in Bear Trap was unexpected, given the small LAI reduction of 8%. The dry years (2012-2013) in Bear Trap had precipitation comparable to the average year (2010) in Big Sandy, where vegetation is water limited. The response at Bear Trap suggests that the vegetation in the higher-precipitation central Sierra is not water limited. Precipitation at Bear Trap met the subsurface-storage and evapotranspiration demand in all years, with excess water from reduced evapotranspiration going to runoff. The runoff increase in response to the biomass reduction was relatively constant (12-14 cm) across wet and dry years. Snowpack and subsurface water availability during the dry years did not persist as far into the spring and summer as it did during the wetter years. As a result, increased water availability from the vegetation reduction largely occurred during the winter period when evapotranspiration is lowest, instead of during the spring period when higher evapotranspiration occurs, leading to the higher runoff response.

In contrast for Big Sandy, thinning impacts on LAI were small, and modeling showed no substantial change in runoff. Lower sensitivity of the water-balance response to vegetation density in Big Sandy may also reflect a greater sensitivity to water limitation, and thus the lower precipitation rates in this area may limit responses of runoff and evapotranspiration to vegetation thinning.

Running and Coughlan [1988] show that in their biogeochemical model, Forest-BGC, changes in LAI scale directly with vegetative water use in areas that are not limited by water availability (*e.g.* Bear Trap), but a similar (or larger) variation in LAI may not show a response in more water-limited ecosystems (*e.g.* Big Sandy). Our model replicated this dependence on water availability, but it also explicitly tracked the effect of changing vegetation structure on the water cycle through changes in

evapotranspiration. Moreover, it translates the impact of these eco-hydrologic responses to streamflow in catchments with different geologies. The model also captured seasonality at both sites and key spatial differences between the two sites (e.g. greater water limitation in Merced R. sites).

4.3 Model uncertainty

Exploring the source of uncertainty can help to improve subsequent use of this measurement and modeling approach to estimate hydrologic response to forest thinning. Hydro-ecologic model uncertainty originates from: *i*) observations of precipitation, temperature, snow, soil moisture and streamflow used for input and calibration, *ii*) model structure and algorithms, and *iii*) equifinality of model parameters.

In this study, the distributed measurements of snow depth and soil moisture were designed to characterize the spatial variability of observations, and thus reduce the uncertainty of those key state variables. For the 2 modeled catchments, the observed timing of catchment-wide snowmelt and streamflow patterns were consistent, and we view this as an improvement over calibrating using snow accumulation inferred from total precipitation. Similarly, the observed basin-wide recession of soil-moisture storage was consistent with streamflow timing.

Surface temperatures vary considerably in mountains [*Cantlon*, 1953; *Fridley*, 2009], as much as 10^{o}C between north- and south-facing slopes on open ground [*Parker*, 1952] as referenced in the MTN-CLIM manuscript [*Running et al.*, 1987]). Adjustments for LAI and aspect incorporated to the MTN-CLIM meteorological drivers of the RHESSys model attempt to account for these variations, but even the evaluation sites for the meteorological model show a range of seasonal temperature estimates that differed 0.04-3.14^{o}C from observations, despite correlation coefficients consistently around 0.90 [*Running et al.*, 1987].

In the complex terrain of the Sierra Nevada, spatial variability in temperature introduces considerable uncertainty into snow accumulation and melt fluxes, and thus streamflow. This was especially challenging, as the catchments include the rain-snow transition zone. We found that temperature thresholds for rain versus snow precipitation varied from event to event. Using a linear model within RHESSys to determine precipitation phase resulted in very low snowpack estimates, particularly in the American. Comparing temperatures from meteorological stations versus those in the snow-depth sensors showed that the meteorological stations may not be representative of the regional elevation. For example, the mean daily winter temperatures recorded at the lower-elevation meteorological station for the American exceeded the maximum daily temperatures recorded in the adjacent valley of Bear Trap Creek at times in the winter, and valley maximum temperatures exceeded meteorological-station maximums during the summer (Figure 7). The meteorological station is located on a partially open ridge, more exposed to the winter sun, and the valley station is located on the stream bank of the Bear Trap outlet, subject to cold-air-drainage effects and little winter sun exposure, causing the differences in daily temperature range.

It has previously been shown that meteorological-station location and temperature-interpolation methods can significantly affect the success of model calibration [*Garcia et al.*, 2013]. It would be useful to explicitly incorporate spatial characteristics of surface temperatures for better temperature-dependent snowmelt simulation in these rain-snow transition zones. We have presented these data to suggest temperature variability is a factor limiting the accuracy of the modeled snow melt and should be improved for future studies.

Precipitation, evapotranspiration and streamflow, the dominant fluxes in our catchments, are measured in only a few locations in the Sierra Nevada. Precipitation and evapotranspiration are challenging to measure, especially at the spatial scale of hydrologic modeling. Lacking an accurate rain gauge, we followed the conventional practice of model calibration using precipitation inferred from gauges a few km away and streamflow measured in the catchment. Our estimated evapotranspiration in Big Sandy compares well with concurrent multi-year measurements in the Kings River basin [*Bales et al.*, 2011; *Goulden et al.*, 2012], about 60 km southeast at the same elevation. The further north Bear Trap catchment showed higher evapotranspiration, commensurate with its greater vegetation density and precipitation. Our streamflow data, based on continuous stream-stage measurements and rating curves, typical for shorter-term studies where stream-channel

alteration is an issue, have more uncertainty than do measurements at longer-term research sites having control sections on streams [*Hunsaker et al.*, 2012]. In this study, the measurements used to develop our rating curves spanned the range of observed streamflow, with the exception of the highest flows (Figure 7). Over the four years, 93-99% of the streamflow volume occurred within the range of measured discharge used for calculating the rating curves.

Estimations of vegetation structure vary by spatial product, and spatial-data uncertainty associated with the polygon-mapping estimates of LAI and canopy cover may have caused higher than observed snowmelt rates with RHESSys. We tested various changes to the model to better represent snowpack in the heterogeneous dense forest characteristic of catchments, and found that using the index-based radiation calculation for snowmelt provided the best model fit. To capture the observed snowpack persistence and melt timing independently of streamflow calibrations, we set the radiation melt coefficient to 0.40 in the model. *Kustas et al.* [2004] showed that a radiation and temperature index-based snowmelt runoff model could perform as well as an energy-balance model, and better than only using a temperature-index model.

Estimates of vegetation structure and density impact snowpack processes, evapotranspiration amount and timing, and the magnitude of changes to the water balance when disturbance or growth occurs. The canopy-cover estimation used in this study was calculated as the amount of ground directly covered by forest canopy, resulting in more open areas than are provided by spectral estimates. Canopy-cover calculated from the polygons defined in this study and the 2011 National Land Cover Database (NLCD; [*Homer et al.* , 2015]) were highly variable. In Bear Trap, field surveys gave a mean canopy cover of 55% (range 32-70%), compared to a mean of 69% (1-100%) from LiDAR and 62% (54-71%) from NLCD. Respective canopy-cover values for Big Sandy were 55% (0-80%), 52% (0-100%) and 60% (0-97%). Further research into the differences of methods used for model input of forest structure are needed (*e.g. Varhola and Coops*, 2013) as spatial-mapping techniques transition towards higher-resolution products, with applications to the vegetation-hydrology interface.

Using multiple parameter sets that met the calibration criteria addresses issues of parameter equifinality and are useful in projecting a distribution of simulated response to forest thinning. Bear Trap had a smaller range of simulation confidence intervals, reflecting the smaller number of parameter sets and smaller range of parameters in acceptable calibrations (Table 1, Figure 4). The 95% confidence intervals of the simulated Bear Trap water-balance components increased with thinning. The mean annual runoff confidence interval was 5 cm before thinning and 8 cm after thinning. The evapotranspiration confidence interval was 3 cm before thinning and 7 cm after thinning. The response of increased runoff and decreased evapotranspiration to the vegetation thinning, however, exceeded the confidence intervals. Big Sandy had a much wider confidence band, associated with the greater number of acceptable calibrations and greater parameter ranges.

The lack of transferable snowpack simulation to the nearby basins, and unsuccessful adjustment of snowmelt parameters for simulation of stream discharge, shows the challenge of modeling this region on a daily timestep. The majority of discharge occurs in winter and spring, and is driven by intermittent snowmelt periods. Although we achieved acceptable snowpack simulation in the two other basins compared to our measurements, the lack of success in streamflow simulations shows the challenge of constraining models to multiple datasets and the need for concentrating distributed measurements within headwater catchments. The precipitation data used, and observations recorded around the ridge meteorological stations near the study catchments and at the stream outlets may not have accurately represented snow patterns within all headwaters, which is critical for simulating daily discharge.

4.4 Data-based modeling

Silberstein [2006] argues that improved modeling for water resources and land management cannot exist without improved data collection, “because we cannot manage what we do not measure.” The limitations and uncertainties of using models to answer hydrologic questions are well known (*e.g. Renard et al.*, 2010), yet models continue to be used ubiquitously. The approach used in this study, integrating distributed observed datasets to

constrain model parameters, produces a grounded and verifiable tool for evaluating catchment-scale responses to changes in vegetation. Using multiple datasets to constrain modeling may not provide the highest model fit. *Seibert and McDonnell* [2002] comment that lower model efficiencies may be necessary when incorporating multiple sources of data, but can produce a better overall model of catchment behavior. Constraining models to a single observation dataset, such as streamflow, can lead to overfitting of model parameters and result in poor model performance, particularly when there is uncertainty in meteorological input data [*Garcia et al.*, 2013].

Our relatively short study period and high precipitation variability limited the ability of field observations alone to conclusively determine catchment response to fuels reduction. Studies like that reported here will grow in importance as we continue to scale estimates of the water-balance impacts of forest fuels treatments, restoration and wildfire across the highly variable climate and regolith found in the Sierra Nevada and other semi-arid regions. The data-informed modeling used in this research provides the ability to evaluate the changes in vegetation over a greater time period and range of precipitation than was available in the post-thinning year of observation. Thus, modeling can be a useful tool for extending observations, but only provides confident results when constrained by spatially distributed field data on multiple components of the water balance.

5 Conclusions

Model simulations constrained by multiyear spatially distributed water-balance measurements show that a reduction in vegetation from forest thinning has potential to result in a corresponding runoff increase in higher-precipitation areas, such as the American River basin, but not necessarily in more-water-limited regions such as the Merced River basin. Simulated evapotranspiration and runoff were sensitive to the relatively small decreases in vegetation over the range of low to high precipitation rates experienced during the study. These model results provide an initial evaluation on the use of forest thinning for increased water yield in the Sierra Nevada, and suggest low-intensity thinning can be effective in forests that are not water limited. In regions of lower precipitation that have greater forest canopy cover and basal area, higher-intensity thinning covering a greater portion of the catchment may be needed to influence the catchment-scale water balance. The high variability in annual precipitation, combined with low post-thinning precipitation, masked any detectable changes in headwater catchment runoff from fuels reduction. Modeling tools to evaluate catchment response to fuels reduction were necessary to address the challenges of a short study period and high precipitation variability. Using a spatially distributed dataset of snow and soil moisture observations, we were able to develop a well-constrained model using multiple observations for simulating catchment response to vegetation thinning. Using this approach of hydrologic modeling, informed by multiple observed datasets, provides a more confident and useful tool for evaluating catchment response to changes in vegetation than models evaluated only on streamflow.

Acknowledgments and Data

This is a SNAMP publication. The Sierra Nevada Adaptive Management Project (SNAMP) was supported by USDA Forest Service Region 5, USDA Forest Service Pacific Southwest Research Station, US Fish and Wildlife Service, California Department of Water Resources, California Department of Fish and Game, California Department of Forestry and Fire Protection, and the Sierra Nevada Conservancy. This research was also supported by US National Science Foundation, through the Southern Sierra Critical Zone Observatory (EAR-0725097). The authors would like to thank the California Department of Water Resources, US Forest Service, Sierra Nevada Research Institute, and Sierra Nevada Adaptive Management Project personnel for their support and assistance. Thanks to the Associate Editor, C. Luce, for comments and feedback that greatly improved the manuscript. The data used are listed in the references, tables, and online data repository at http://snamp.ucmerced.edu.

References

Agee, J. K., and C. N. Skinner (2005), Basic principles of forest fuel reduction treatments, *For. Ecol. Manage.*, *211*(1–2), 83–96, doi:10.1016/j.foreco.2005.01.034.

Asner, P. A., P. G. Brodrick, C. B. Anderson, N. Vaughn, D. E. Knapp, and R. E. Martin

(2016), Progressive forest canopy water loss during the 2012-2015 California drought, *Proc. Natl. Acad. Sci., 113(2)*, 249-255, doi:10.1073/pnas.1523397113.

Bales, R. C., J. W. Hopmans, A. T. O'Geen, M. Meadows, P. C. Hartsough, P. Kirchner, C. T. Hunsaker, and D. Beaudette (2011), Soil Moisture Response to Snowmelt and Rainfall in a Sierra Nevada Mixed-Conifer Forest, *Vadose Zo. J.*, *10*(3), 786, doi:10.2136/vzj2011.0001.

Barry, R. G., and R. J. Chorley (1987), *Atmosphere, weather and climate*, 5th ed., Routledge, London, UK.

Bateman, P. C. (1989), *Geologic map of the Bass Lake quadrangle, west-central Sierra Nevada, California*, Geologic Quandrangle Map GQ-1656.

Biederman, J., A. Harpold, D. Gochis, B. Ewers, D. Reed, S. Papuga, and P. Brooks (2014), Increased evaporation following widespread tree mortality limits streamflow response, *Water Resour. Res.*, *50*, 5395–5409, doi:10.1002/2013WR014994.

Bosch, J., and J. Hewlett (1982), A review of catchment experiments to determine the effect of vegetation changes on water yield and evapotranspiration, *J. Hydrol.*, *55*, 3–23, doi:10.1016/0022-1694(82)90117-2.

Brubaker, K., A. Rango, and W. Kustas (1996), Incorporating radiation inputs into the snowmelt runoff model, *Hydrol. Process.*, *10*, 1329-1343.

Burt, T. P., and J. J. McDonnell (2015), Whither field hydrology? the need for discovery science and outrageous hydrological hypotheses, *Water Resour. Res.*, *51*(8), 5919–5928, doi:10.1002/2014WR016839.

California Department of Water Resources (2015), Precipitation data for Drum Power House, Hellhole, and Huysink stations, *Calif. Data Exch. Cent.*, 10/1/2009-9/302013. Available from: http://cdec.water.ca.gov/ (Accessed 21 October 2015)

Cantlon, J.E. (1953), Vegetation and microclimates on north and south slopes of Cushetunk Mountain, New Jersey, *Ecol. Monogr., 23(3)*, 241-270, doi:10.2307/1943593.

Chauvin, G. M., G. N. Flerchinger, T. E. Link, D. Marks, A. H. Winstral, and M. S. Seyfried (2011), Long-term water balance and conceptual model of a semi-arid mountainous catchment, *J. Hydrol.*, *400*(1–2), 133–143, doi:10.1016/j.jhydrol.2011.01.031.

Collins, B. M., R. G. Everett, and S. L. Stephens (2011), Impacts of fire exclusion and recent managed fire on forest structure in old growth Sierra Nevada mixed-conifer forests, *Ecosphere*, *2*(4), 14, doi:10.1890/ES11-00026.1.

Conklin, M., R. Bales, P. Saksa, S. Martin, and R. Ray (2015), Appendix E – Water Team Report *in Learning adaptive management of Sierra Nevada forests: An integrated assessment* (Hopkinson, P. and Battles, J.J., eds.). Center for Forestry, University of California, Berkeley.

Corbari, C., M. Mancini, J. Li, and Z. Su (2015), Can satellite land surface temperature data be used similarly to river discharge measurements for distributed hydrological model calibration?, *Hydrol. Sci. J.*, *60*(2), 202–217, doi:10.1080/02626667.2013.866709.

Cornwall, E., N. P. Moloth, and J. McPhee (2016), Spatio-temporal varaibility of snow water equivalent in the extra-tropical Andes Cordillera from distributed energy balance modeling and remotely sensed snow cover, *Hydrol. Earth Syst. Sci. 20*, 411-430, doi:10.5194/hess-20-411-2016.

Coughlan, J. W., and S. W. Running (1997), Regional ecosystem simulation: A general model for simulating snow accumulation and melt in mountainous terrain, *Land. Ecol., 12*, 119-136, doi:10.1023/A:1007933813251.

Crookston, N. L., and A. R. Stage (1999), Percent canopy cover and stand structure statistics from the Forest Vegetation Simulator, *USDA For. Serv. Rocky Mt. Res. Stn., RMRS-GTR-2*.

Dunne, T. (1983), Relation of field studies and modeling in the prediction of storm runoff, *J. Hydrol.*, *65*(1–3), 25–48, doi:10.1016/0022-1694(83)90209-3.

Essery, R., J. Pomeroy, C. Ellis, and T. Link (2008), Modelling longwave radiation to snow beneath forest canopies using hemispherical photography or linear regression, *Hydrol. Process.*, *22*(15), 2788–2800.

Fellows, A.W., and M. L. Goulden (2016),

Mapping and understanding dry season soil water drawdown by California montane vegetation, *Ecohydrol.*, doi:10.1002/eco.1772.

Ffolliott, P. F., G. J. Gottfried, and M. B. Baker (1989), Water Yield From Forest Snowpack Management: Research Findings in Arizona and New Mexico, *Water Resour. Res.*, *25*(9), 1999–2007, doi:10.1029/WR025i009p01999.

Finney, M. (2001), Design of regular landscape fuel treatment patterns for modifying fire growth and behavior, *For. Sci.*, *47*(2), 219–228.

Fridley, J.D. (2009), Downscaling Climate over Complex Terrain: High Finescale (<1000 m) Spatial Variation of Near-Ground Temperatures in a Montane Forested Landscape (Great Smoky Mountains), *J. Appl. Meteor. and Clim.*, *48(5)*, 1033-1049, doi:10.1175/2008JAMC2084.1.

Fry, D., J. Battles, B. Collins, and S. Stephens (2015), Appendix A – Fire and Forest Ecosystem Health Report *in Learning adaptive management of Sierra Nevada forests: An integrated assessment* (Hopkinson, P. and Battles, J.J., eds.). Center for Forestry, University of California, Berkeley.

Garcia, E. S., C. L. Tague, and J. S. Choate (2013), Influence of spatial temperature estimation method in ecohydrologic modeling in the Western Oregon Cascades, *Water Resour. Res.*, *49*(3), 1611–1624, doi:10.1002/wrcr.20140.

Garcia, E. S., C.L. Tague (2015), Subsurface storage capacity influences climate-evapotranspiration interactions in three western United States catchments, *Hydrol. Earth Syst. Sci.*, *19*, 4845-4858, doi:10.5194/hess-19-4845-2015.

Goulden, M. L., R. G. Anderson, R. C. Bales, A. E. Kelly, M. Meadows, and G. C. Winston (2012), Evapotranspiration along an elevation gradient in California's Sierra Nevada, *J. Geophys. Res.*, *117*(G3), G03028, doi:10.1029/2012JG002027.

Grayson, R. B., I. D. Moore, and T. A. McMahon (1992), Physically based hydrologic modeling 2. Is the concept, *Water Resour Res*, *26*(10), 2659–66.

Grayson, R. B., G. Blöschl, A. W. Western, and T. a McMahon (2002), Advances in the use of observed spatial patterns of catchment hydrological response, *Adv. Water Resour.*, *25*(8–12), 1313–1334, doi:10.1016/S0309-1708(02)00060-X.

Griffen, D., and K. J. Anchukaitis (2014), How unusual is the 2012-2014 California drought?, *Geophys. Res. Lett. 41*, 9017-9023, doi:10.1002/2014GL062433.

Guan, B. N. P. Molotch, D. E. Waliser, E. J. Fetzer, and P. J. Neiman (2013), The 2010/2011 snow season in California's Sierra Nevada: Role of atmospheric rivers and modes of large-scale variability, *Water Resour. Res.*, *49*, 6731-6743, doi:10.1002/wrcr.20537.

Hicks, B. J., R. L. Beschta, and R. D. Harr (1991), Long-Term Changes in Streamflow Following Logging in Western Oregon and Associated Fisheries Implications, *J. Am. Water Resour. Assoc.*, *27*(2), 217–226, doi:10.1111/j.1752-1688.1991.tb03126.x.

Holbrook, W.S., C.S. Riebe, M. Elwaseif, J.L. Hayes, K. Basler-Reeder, D.L. Harry, A. Malazian, A. Dosseto, P.C. Hartsough, and J.W. Hopmans (2014), Geophysical constraints on deep weathering and water storage potential in the Southern Sierra Critical Zone Observatory, *Earth Surf. Process. Landforms*, *39*, doi:10.1002/esp.3502.

Homer, C. G., J. A. Dewitz, L. Yang, S. Jin, P. Danielson, G. Xian, J. Coulston, N. D. Herold, J. D. Wickham, and K. Megown (2015), Completion of the 2011 National Land Cover Database for the conterminous United States-Representing a decade of land cover change information, *Photogramm. Eng. Remote Sensing*, *81*(5), 345–354, doi:10.14358/PERS.81.5.345.

Hungerford, R. D., R. R. Nemani, S. W. Running, and J. C. Coughlan (1989), *MTCLIM : A Mountain Microclimate Simulation Model; INT-414*, Ogden, UT.

Hunsaker, C. T., T. W. Whitaker, and R. C. Bales (2012), Snowmelt Runoff and Water Yield Along Elevation and Temperature Gradients in California's Southern Sierra Nevada, *J. Am. Water Resour. Assoc.*, *48*(4), 667–678, doi:10.1111/j.1752-1688.2012.00641.x.

Jones, D., K. O'Hara, J. Battles, and R. Gersonde (2015), Leaf Area Prediction Using

Three Alternative Sampling Methods for Seven Sierra Nevada Conifer Species, *Forests*, *6*(8), 2631–2654, doi:10.3390/f6082631.

Kattelmann, R. C., N. H. Berg, and J. Rector (1983), the Potential for Increasing Streamflow From Sierra Nevada Watersheds, *J. Am. Water Resour. Assoc.*, *19*(3), 395–402, doi:10.1111/j.1752-1688.1983.tb04596.x.

Kittredge, J. (1953), Influences of forests on snow in the ponderosa-sugar pine-fir zone of the Central Sierra Nevada, *Hilgardia*, *22*(1), 1–96.

Klemes, V. (1986), Dilettantism in hydrology: Transition or destiny?, *Water Resour. Res.*, *22*(9), 177S–188S, doi:10.1029/WR022i09Sp0177S.

Kustas, W., A. Rango, and R. Uijlenhoet (1994), A simple energy budget algorithm for the snowmelt runoff model, *Water Resour. Res. 30(5)*, 1515-1527, doi:10.1029/94WR00152.

Lawler, R. R., and T. E. Link (2011), Quantification of incoming all-wave radiation in discontinuous forest canopies with application to snowmelt prediction, *Hydrol. Process.*, doi:10.1002/hyp.8150.

Liu, F., C. Hunsaker, and R. C. Bales (2013), Controls of streamflow generation in small catchments across the snow-rain transition in the Southern Sierra Nevada, California, *Hydrol. Process.*, *27*(14), 1959–1972, doi:10.1002/hyp.9304.

Lundquist, J. D., S. E. Dickerson-Lange, J. A. Lutz, and N. C. Cristea (2013), Lower forest density enhances snow retention in regions with warmer winters: A global framework developed from plot-scale observations and modeling, *Water Resour. Res.*, *49*(4), doi:10.1002/wrcr.20504.

Luo, Y., D. L. Ficklin, X. Liu, and M. Zhang (2013), Assessment of climate change impacts on hydrology and water quality with a watershed modeling approach, *Sci. Total Environ.*, *450–451*, 72–82, doi:10.1016/j.scitotenv.2013.02.004.

Marvin, S. (1996), Possible changes in water yield and peak flows in response to forest management, in *Sierra Nevada Ecosystem Project: Final Report to Congress*, vol. 101, pp. 154–199.

Moore, G. W., B. J. Bond, J. A. Jones, N. Phillips, and F. C. Meinzer (2004), Structural and compositional controls on transpiration in 40- and 450-year-old riparian forests in western Oregon, USA., *Tree Physiol.*, *24*(5), 481–91.

Moore, R. D. (2013), Introduction to salt dilution gauging for streamflow measurement Part 3: Slug injection using salt in solution, *Streamline Watershed Manag. Bull.*, *7*(4), 20–23, doi:10.1592/phco.23.9.1S.32890.

Nash, J. E., and J. V Sutcliffe (1970), River flow forecasting through conceptual models part I -- A discussion of principles, *J. Hydrol.*, *10*(3), 282–290.

North, M., J. Innes, and H. Zald (2007), Comparison of thinning and prescribed fire restoration treatments to Sierran mixed-conifer historic conditions, *Can. J. For. Res.*, *37*(2), 331–342, doi:10.1139/X06-236.

Ohmann, J. L., and M. J. Gregory (2002), Predictive mapping of forest composition and structure with direct gradient analysis and nearest- neighbor imputation in coastal Oregon, U.S.A., *Can. J. For. Res.*, *32*(4), 725–741, doi:10.1139/x02-011.

Parker, J. (1952), Environment and Forest Distribution of the Palouse Range in Northern Idaho, *Ecology*, *33*(4), 451–461.

Renard, B., D. Kavetski, G. Kuczera, M. Thyer, and S. W. Franks (2010), Understanding predictive uncertainty in hydrologic modeling: The challenge of identifying input and structural errors, *Water Resour. Res.*, *46*(5), 1–22, doi:10.1029/2009WR008328.

Rowe, P., and T. Hendrix (1951), Interception of rain and snow by second-growth ponderosa pine, *Trans. Amer. Geophys. Union*, *32*(6), 903–908.

Running, S., and J. Coughlan (1988), A General Model of Forest Ecosystem Processes for regional applications I. Hydrologic balance, canopy gas exchange and primary production processes., *Ecol. Modell.*, *42*, 125–154.

Running, S. W., R. R. Nemani, and R. D. Hungerford (1987), Extrapolation of synoptic meteorological data in mountainous terrain and its use for simulating forest evapotranspiration and photosynthesis, *Can. J. For. Res.*, *17*(6), 472–483.

Saucedo, G. J., and D. L. Wagner (1992), *Geologic Map of the Chico quadrangle*, Regional Geologic Map 7A.

Seibert, J., and J. J. McDonnell (2002), On the dialog between experimentalist and modeler in catchment hydrology: Use of soft data for multicriteria model calibration, *Water Resour. Res.*, *38*(11), 23, 1–14, doi:10.1029/2001WR000978.

Shaw, G. D., M. H. Conklin, G. J. Nimz, and F. Liu (2014), Groundwater and surface water flow to the Merced River, Yosemite Valley, California: ^{36}Cl and Cl^- evidence, *Water Resour. Res.*, *50*, 1943–1959, doi:10.1002/2013WR014222.

Silberstein, R. P. (2006), Hydrological models are so good, do we still need data?, *Environ. Model. Softw.*, *21*(9), 1340–1352, doi:10.1016/j.envsoft.2005.04.019.

Soil Survey Staff (2011), *Soil Survey Geographic (SSURGO) Database*. Natural Resources Conservation Service, United States Department of Agriculture.

Son, K., C. Tague, and C. Hunsaker (2016), Effects of model spatial resoluation on ecohydrologic predictions and their sensitivity to inter-annual climate variability, *Water*, *8(8)*, doi:10.3390/w8080321.

Stednick, J. (1996), Monitoring the effects of timber harvest on annual water yield, *J. Hydrol.*, *176*(1–4), 79–95, doi:10.1016/0022-1694(95)02780-7.

Storck, P., D. P. Lettenmaier, and S. M. Bolton (2002), Measurement of snow interception and canopy effects on snow accumulation and melt in a mountainous maritime climate, Oregon, United States, *Water Resour. Res.*, *38*(11), 1123.

Su, Y., Q. Guo, D. L. Fry, B. M. Collins, M. Kelly, J. P. Flanagan, and J. J. Battles (2016), A Vegetation Mapping Strategy for Conifer Forests by Combining Airborne LiDAR Data and Aerial Imagery, *Can. J. Remote Sens.*, *42*, 1-15, doi:10.1080/07038992.2016.1131114.

Sun, G., P. V. Caldwell, and S. G. McNulty (2015), Modeling the potential role of forest thinning in maintaining water supplies under a changing climate across the Conterminous United States, *Hydrol. Process.*, doi:10.1002/hyp.10469.

Swank, W., J. Vose, and K. Elliott (2001), Long-term hydrologic and water quality responses following commercial clearcutting of mixed hardwoods on a southern Appalachian catchment, *For. Ecol. Manage.*, *143*, 163–178, doi:10.1016/S0378-1127(00)00515-6.

Tague, C., and G. E. Grant (2004), A geological framework for interpreting the low-flow regimes of Cascade streams, Willamette River Basin, Oregon, *Water Resour. Res.*, *40*(4), 1–9, doi:10.1029/2003WR002629.

Tague, C., and H. Peng (2013), The sensitivity of forest water use to the timing of precipitation and snowmelt recharge in the California Sierra: Implications for a warming climate, *J. Geophys. Res. Biogeosciences*, *118*, n/a-n/a, doi:10.1002/jgrg.20073.

Tague, C. L., and L. E. Band (2004), RHESSys: Regional Hydro-Ecologic Simulation System—An Object-Oriented Approach to Spatially Distributed Modeling of Carbon, Water, and Nutrient Cycling, *Earth Interact.*, *8*(19), doi:http://dx.doi.org/10.1175/1087-3562(2004)8<1:RRHSSO>2.0.CO;2.

Tague, C. L., J. S. Choate, and G. Grant (2013), Parameterizing sub-surface drainage with geology to improve modeling streamflow responses to climate in data limited environments, *Hydrol. Earth Syst. Sci.*, *17*(1), 341–354, doi:10.5194/hess-17-341-2013.

Troendle, C. A., and R. M. King (1985), The effect of timber harvest on the Fool Creek watershed, 30 years later, *Water Resour. Res*, *21*(12), 1915–1922.

Troendle, C. A., M. S. Wilcox, G. S. Bevenger, and L. S. Porth (2001), The Coon Creek Water Yield Augmentation Project: implementation of timber harvesting technology to increase streamflow, *For. Ecol. Manage.*, *143*, 179–187, doi:10.1016/S0378-1127(00)00516-8.

Varhola, A., and N. C. Coops (2013), Estimation of watershed-level distributed forest structure metrics relevant to hydrologic modeling using LiDAR and Landsat, *J. Hydrol.*, *487*, 70–86, doi:10.1016/j.jhydrol.2013.02.032.

Vicente-Serrano, S. M., J. J. Camarero, J. Zabalza, G. Sanguesa-Barreda, J. I. Lopez-Moreno, and C. L. Tague (2015), Evapotranspiration deficit controls net primary production and growth of silver fir: Implications for Circum-Mediterranean forests under forecasted warmer and drier conditions, *Agric. For. Meteorol.*, *206*, 45–54, doi:10.1016/j.agrformet.2015.02.017.

Wayman, R. B., and M. North (2007), Initial

response of a mixed-conifer understory plant community to burning and thinning restoration treatments, *For. Ecol. Manage.*, *239*(1–3), 32–44, doi:10.1016/j.foreco.2006.11.011.

Westerberg, I. K., T. Wagener, G. Coxon, H. K. McMillan, A. Castellarin, A. Montanari, and J. Freer (2016), Uncertainty in hydrological signatures for gauged and ungauged catchments, *Water Resour. Res.*, *52*(3), 1847–1865, doi:10.1002/2015WR017635.

Whitehead, D., and F. M. Kelliher (1991), A canopy water balance model for a {\em Pinus radiata} stand before and after thinning, *Agric. For. Meteo.*, *55*, 109–126, doi:10.1016/0168-1923(91)90025-L.

Whitehead, D., P. G. Jarvis, and R. H. Waring (1984), Stomatal conductance, transpiration, and resistance to water uptake in a Pinus sylvestris spacing experiment, *Can. J. For. Res.*, (14), 692–700.

Zhang, L., W. R. Dawes, and G. R. Walker (2001), Response of mean annual evapotranspiration to vegetation changes at catchment scale, *Water Resour. Res.*, *37*(3), 701–708.

Zierl, B., H. Bugmann, and C. L. Tague (2007), Water and carbon fluxes of European ecosystems: an evaluation of the ecohydrological model RHESSys, *Hydrol. Process.*, *21*, 3328–3339, doi:10.1002/hyp.

Zou, C. B., P. F. Ffolliott, and M. Wine (2010), Streamflow responses to vegetation manipulations along a gradient of precipitation in the Colorado River Basin, *For. Ecol. Manage.*, *259*(7), 1268–1276, doi:10.1016/j.foreco.2009.08.005.

Table 1. Calibrated model parameter ranges and streamflow fit statistics[1] for Bear Trap and Big Sandy catchments.

Parameter	Description	Range	Bear Trap	Big Sandy
m	decay of hydraulic conductivity with depth, dimensionless	0 - 20	5.6 – 12.3	0.6 – 19.9
k	Surface lateral hydraulic conductivity, m day^{-1}	0 - 300	2.0 – 6.6	5 - 294
svk	Surface vertical hydraulic conductivity, m day^{-1}	0 - 300	7 – 250	2 – 294
po	soil pore size index, dimensionless	0 - 3	1.4 – 3.0	0.1 – 3.0
pa	soil air entry pressure, m	0 - 3	0.6 – 2.6	0.2 – 2.9
gw1	groundwater bypass flow, dimensionless	0 - 0.4	0.0 – 0.15	0.2 – 0.4
gw2	Groundwater drainage rate , dimensionless	0 - 0.4	0.0 – 0.01	0.1 – 0.4
NS_e	Nash-Sutcliffe Efficiency	0.60 – 1.00	0.60 – 0.64	0.67 – 0.78
$logNS_e$	Nash-Sutcliffe Efficiency of log-transformed streamflow	0.60 – 1.00	0.75 – 0.84	0.62 – 0.70
ERR_{str}	Annual streamflow error	-0.20 – 0.20	0.00 – 0.17	-0.20 – 0.06
ERR_{aug}	August streamflow error	-0.25 – 0.25	-0.18 – 0.23	-0.19 – 0.12

[1]Model statistics of Nash-Sutcliffe Efficiency for streamflow (NS_e>0.6), NS_e for log-transformed streamflow ($logNS_e$>0.6), annual streamflow error (ERR_{str}<0.2), and August streamflow error (ERR_{aug}<0.25) were used to determine acceptable parameter sets.

Table 2. Interannual variability of precipitation (P), runoff (Q), and loss (P-Q) through evapotranspiration and subsurface drainage observed in the study catchments.[1]

Catchment	Year	P, cm	Q, cm	P-Q, cm	Q/P	(P-Q)/P
Bear Trap	2010	191	67	124	0.35	0.65
	2011	275	134	141	0.49	0.51
	2012	160	41	119	0.26	0.74
	2013	169	43	126	0.25	0.75
Frazier	2010	191	88	103	0.46	0.54
	2011	275	167	108	0.61	0.39
	2012	160	62	98	0.39	0.61
	2013	169	44	125	0.26	0.74
Big Sandy	2010	152	52	100	0.34	0.66
	2011	202	112	90	0.55	0.45
	2012	83	23	60	0.28	0.72
	2013	85	29	56	0.34	0.66
Speckerman	2010	152	39	113	0.26	0.74
	2011	202	77	125	0.38	0.62
	2012	83	24	59	0.29	0.71
	2013	85	31	54	0.36	0.64

[1]Runoff fraction (Q/P) and loss fraction ((P-Q)/P) are calculated as the fraction of precipitation by water year, and include a mean precipitation year (2010), wet year (2011), and two dry years (2012-13).

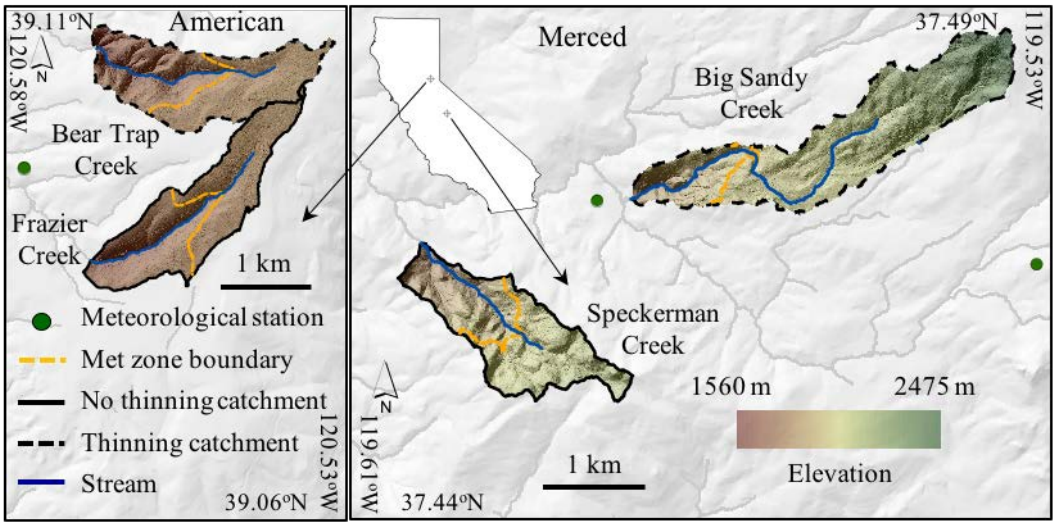

Figure 1. Locations of the headwater research catchments in the American and Merced River basins. The upper elevation meteorological station in the American is located off the map, 8.8 km northeast of the lower-elevation station shown above. The met zone boundary shows the delineation between upper and lower meteorological stations used for determining climate zones in the RHESSys model. Coordinates are in decimal degrees and elevation-band colors apply to all catchments.

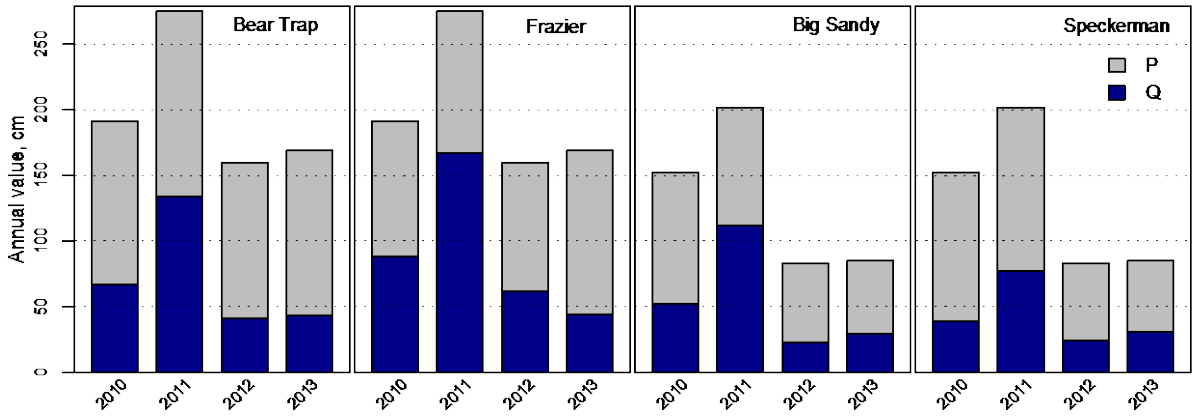

Figure 2. Interannual variability of precipitation (P) and runoff (Q) observed during the four-year study. The height of each bar represents total precipitation, and the blue section of the bar indicates the portion of precipitation measured as runoff in each catchment. Precipitation amounts are the same for Bear Trap and Frazier in the American River and for Big Sandy and Speckerman in the Merced River. Water years 2010 to 2012 are pre-thinning and 2013 is the post-thinning year.

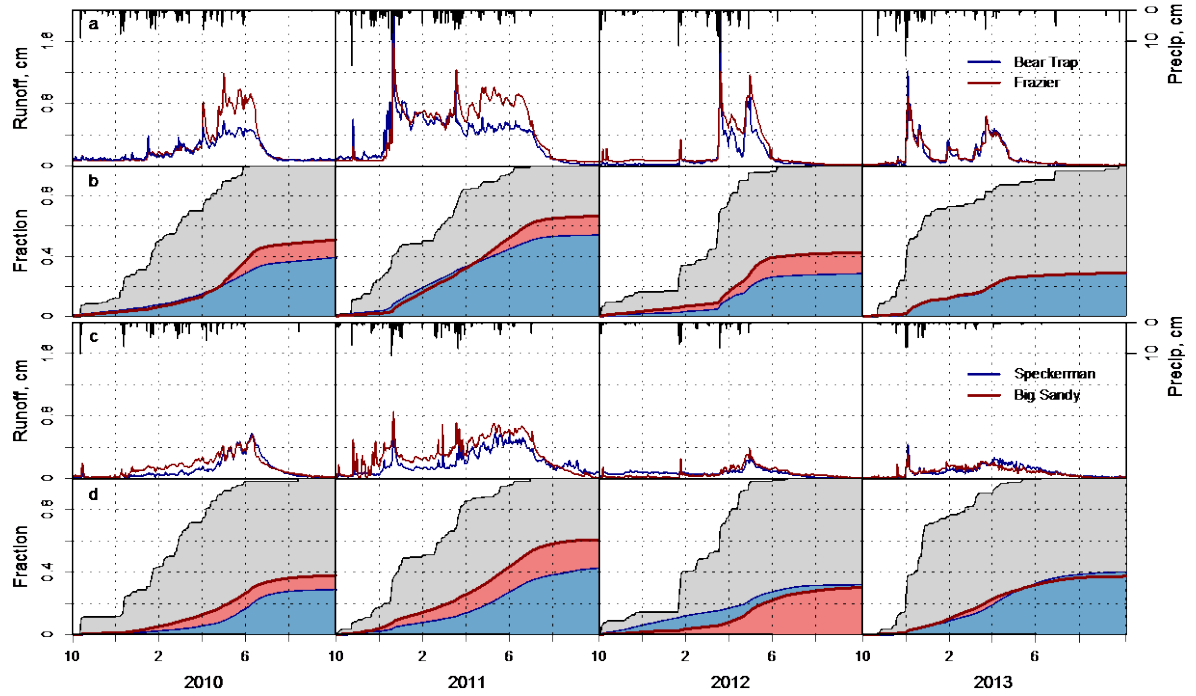

Figure 3. Daily (a,c) and cumulative (b,d) precipitation and runoff observations for the American and Merced River sites during water years (October through September) 2010-2013. Cumulative precipitation and runoff panels (b,d) show the daily increases of the water balance components over the water year. Black lines show mean of distributed snow and soil-water observations; shaded area shows one standard deviation.

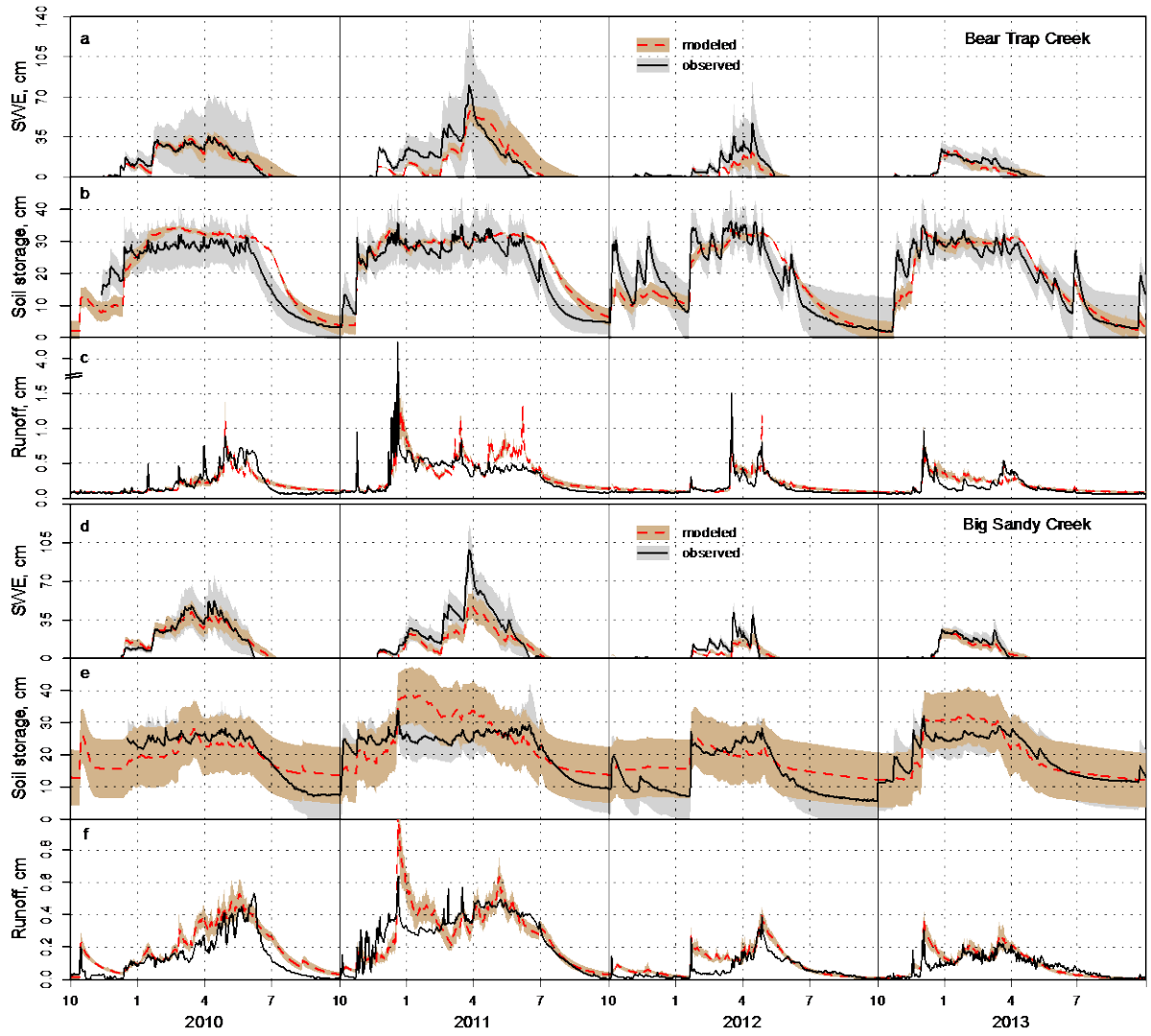

Figure 4. Model daily output of snow water equivalent (SWE) (a,d), root zone soil storage in the top 1-m (b,e), and stream discharge (c,f) compared to mean observation values in Bear Trap (American River, top panel) and Big Sandy (Merced River, bottom panel) catchments. The shaded area of modeled SWE represents the range of radiation coefficients for snowmelt from 0.3 to 0.5, with the line showing the snowpack at the 0.4 radiation coefficient used for all simulations. Shaded areas for all other data represent one standard deviation from the mean, with model mean and standard deviations from the sets of calibrated parameters.

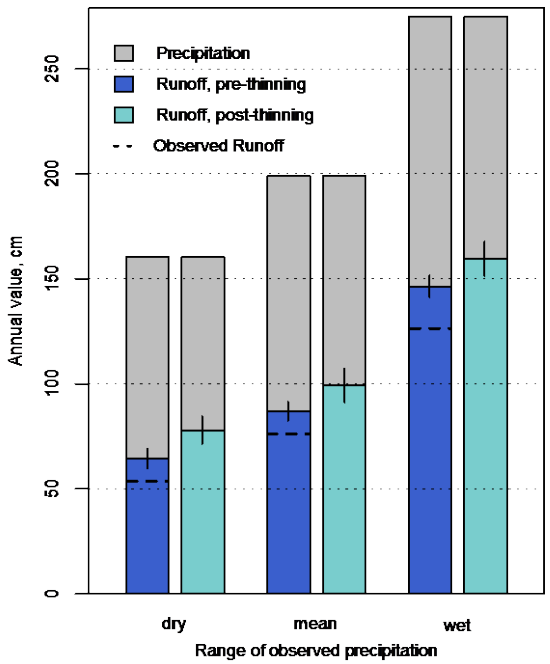

Figure 5. Modeled thinning effects on the water balance in Bear Trap (American River) over the range of observed annual precipitation rates. Runoff increased 21% in the driest year (2012), 14% over the mean from all four years of observations (2010-2013), and 9% in the wettest year (2011). Simulated discharge in the pre-thinning scenarios exceeded observed discharge by 15-20%. Vertical bars indicate 95% confidence intervals of simulated annual runoff from the multiple sets of calibrated parameters.

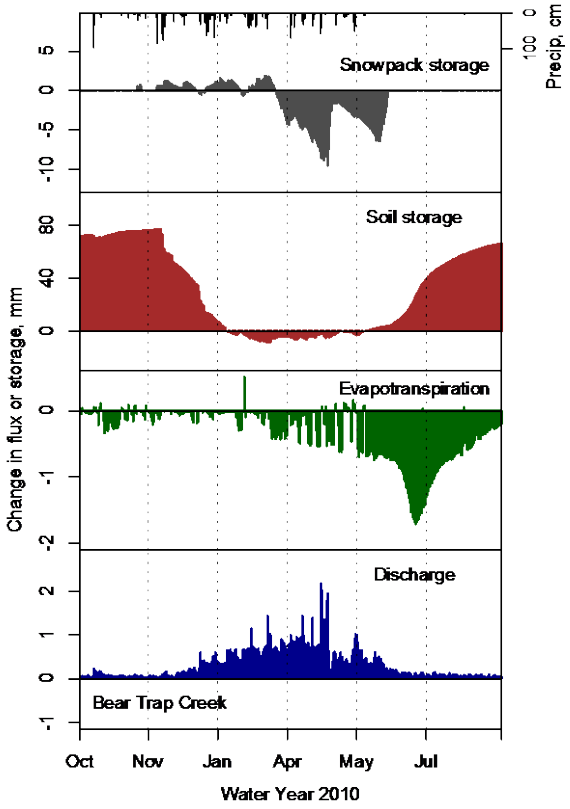

Figure 6. Changes in daily snowpack storage, soil water storage, evapotranspiration, and discharge modeled for the Bear Trap catchment after forest thinning. Panels show the difference in water balance components modeled with pre- and post-thinning vegetation conditions during an average precipitation year (2010).

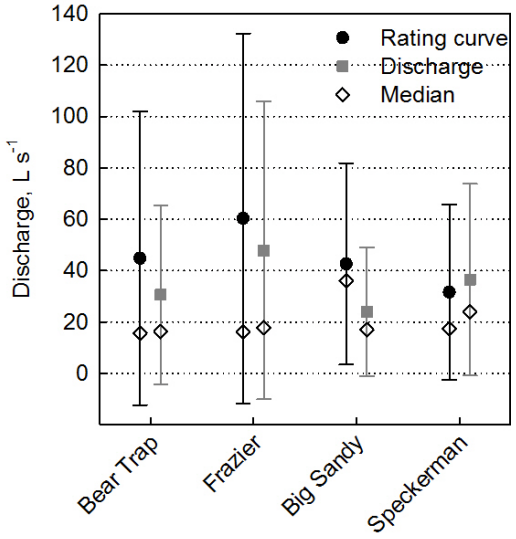

Figure 7. Mean, standard deviation and median of rating-curve and stream-discharge measurements for the 4 study catchments. The number of rating-curve measurements for Bear Trap, Frazier, Big Sandy, and Speckerman were 24, 21, 24 and 16, respectively.

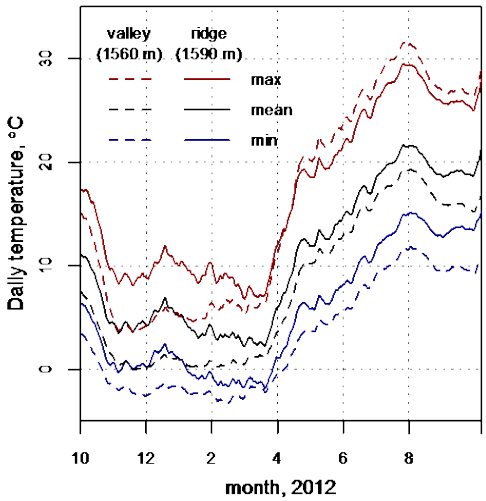

Figure 8. Distributed sensors show ridge temperatures recorded at the meteorological station used for hydrologic model input may not capture the temperature characteristics recorded by the snow depth sensor in the valley. Shaded areas highlight the temperature differences and daily values are smoothed using a running 30-day mean.